Robust Class E^2 Wireless Power Transfer System Based on Parity–Time Symmetry

Liangzong He, *Member, IEEE*, Xiayi Huang, and Bing Cheng

***Abstract*—Thanks to the superiority of zero-voltage switching (ZVS), the Class E^2 topology has become a promising candidate in wireless power transfer (WPT) at medium and small power levels. However, in practical applications, it is a challenging and significant issue to maintain robust WPT under varying transfer distances, especially for the highly sensitive Class E power amplifier (PA). To solve this issue, the parity–time (PT) theory is initially developed into the Class E^2 WPT system. A general design procedure for the PT-symmetry-based Class E^2 WPT system is proposed, including the parameters of the Class E PA, resonant tank, and Class E rectifier. The power losses and efficiencies of the above-mentioned components are analytically derived as well. The ZVS operation is quantitatively described for the PT-symmetry-based Class E^2 WPT system, demonstrating that the maximum phase variation with coupling coefficient is rather small and independent of the natural resonant frequency, thereby achieving robust and highly efficient power transfer. Finally, the prototype with current feedback control to guarantee the PT mechanism and ZVS is built. The experimental results illustrate that under various coupling coefficients, robust and efficient power transfer is realized by a 165-W prototype with about 92.6% efficiency.**

***Index Terms*—Class E^2 topology, parity–time symmetry, wireless power transfer (WPT), zero-voltage switching (ZVS).**

I. Introduction

THE research wave toward wireless power transfer (WPT) has been raised once again across the world since a research team led by Prof. M. Soljacic of MIT made a breakthrough in middle-range WPT in 2007 [1]. In recent years, the main progress of WPT concentrates on the improvement of transfer distance, system efficiency, output power, and dynamic characteristics [2], [3], [4], [5], [6], [7], [8], [9], [10], [11], [12], [13], [14], [15], [16], [17], [18], [19], [20]. The distance and efficiency between the transmitting and receiving coils in WPT systems can be improved with an increase in the operating frequency in a certain range. To operate at a higher frequency, both the inverter and rectifier are required to achieve a soft-switching state to reduce losses, which has attracted considerable attention to the Class E^2 topology, i.e., the Class E power amplifier (PA) and the Class E rectifier.

The critical defect of the Class E PA is that only under or suboptimum operating conditions, its zero-voltage switching (ZVS) can be reached. As a consequence, many research groups revolve around designing the parameters and optimizing the subsystems to achieve higher system efficiency. In [3], an analytical design procedure for each component of a Class E^2 WPT system was presented. In [4], the input impedance of the Class E rectifier was accurately derived and used to design optimal parameters for an MHz WPT system. By applying a numerical design algorithm, an efficient WPT system with multiple receivers was designed in [5]. Chen et al. [6] replaced the parasitic capacitance of the transistor with the charging capacitance to achieve higher system efficiency. An efficient Class E driver was realized in [7] to reduce the gate-drive power for MHz WPT applications.

In WPT systems, it is desirable to realize robust and efficient power transfer to reduce the waste of charging capacity and extend the battery life. Meanwhile, owing to the inevitable variation of the coupling coefficient, system output will suffer a drastic drop in practical applications. For Class E^2 WPT systems, the above-mentioned problem is aggravated due to the sensitive Class E PA. Accordingly, some research teams center on the analysis and design of Class E^2 WPT systems with variable coupling coefficients. A steady-state analysis of a Class E^2 WPT system outside nominal operation was raised in [8], and a design procedure for Class E PA achieving ZVS at any coupling coefficient was introduced in [9]. In [10], an active Class E rectifier with output voltage regulation was developed, which can maintain a stable output voltage under a range of coupling coefficients. An active switched-capacitor Class E rectifier was proposed in [11] to achieve constant output voltage under varying operating conditions. However, the efficiency of the aforementioned Class E rectifier is still reduced with an increasing coupling coefficient. In [12], a harmonic injection method was utilized on a Class E PA for ZVS with various coupling coefficients. A robust impedance matching network (IMN) and a tunable IMN were respectively established in [13] and [14] to improve the robustness of Class E^2 WPT systems. Nevertheless, additional circuits are required in [12], [13], and [14], and the design methods of the latter two were complicated.

Thanks to Assawaworrarit et al. [15], the interdisciplinary integration of parity–time (PT) symmetry and WPT initiates the

Manuscript received 4 November 2022; accepted 15 December 2022. Date of publication 20 December 2022; date of current version 14 February 2023. This work was supported in part by the National Natural Science Foundation Project under Grant 62071406 and in part by Guangdong Province Natural Science Foundation under Grant 2021A1515011710. Recommended for publication by Associate Editor M. Vitelli. *(Corresponding authors: Liangzong He; Xiayi Huang.)*

Liangzong He and Bing Cheng are with the Department of Electrical Engineering, Xiamen University, Xiamen 361102, China (e-mail: hlz190213@163.com; 1606912765@qq.com).

Xiayi Huang is with the Department of Electrical Engineering, Tongji University, Shanghai 200000, China (e-mail: xiayihuang@tongji.edu.cn).

This article has supplementary material provided by the authors and color versions of one or more figures available at https://doi.org/10.1109/TPEL.2022.3230852.

Digital Object Identifier 10.1109/TPEL.2022.3230852

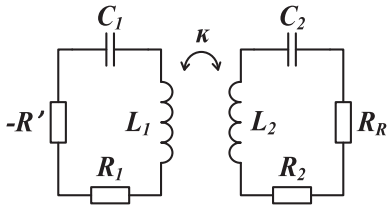

Fig. 1. CMT model of the PT-symmetry-based WPT system.

feasibility of self-robust WPT systems. Originating from quantum physics, PT symmetry implies the balance between gain and loss under parity and time-reversal operations. By establishing a PT-symmetric WPT system, robust and efficient power is automatically guaranteed. Yet, the saturable gain element employed in [15] to track PT symmetry was an operational amplifier, whose intrinsic loss resulted in extremely low output (around 19.7 mW of power and less than 10% of system efficiency). With the rise of switch-mode power electronics, half-bridge and full-bridge inverters replaced the inefficient operational amplifier for higher efficiency and power [16], [17], [18], [19]. However, the conventional half-bridge and full-bridge topologies are hard-switching topologies, causing the need for extra soft-switching control circuits. Besides, the transfer efficiency not only includes the conversion loss, like switching loss or conduction loss, but also depends on the impedance match and energy coupling between the transmitter and receiver resonators. Hence, the traditional topologies may exhibit the same transfer performance in terms of constant transfer efficiency and power while suffering from lower efficiency at the same output power. In comparison, the Class E^2 topology has received more attention during high-frequency, low-/medium-power WPT applications because it employs only one active switch and one diode and enjoys inherent ZVS, zero derivative switching (ZDS), no shoot-through problem, and a simple driving circuit. Therefore, this article proposes a PT-symmetry-based Class E^2 WPT system with robust and efficient output against varying coupling coefficients. Our work extends from the previous works [16], [17], [18], [19], [20] in the following aspects.

1) A universal design methodology for the PT-symmetry-based Class E^2 WPT system is established, guiding other WPT systems with mirror-symmetric oscillators between the transmitter and receiver.
2) The power losses and efficiencies of each part of the PT-symmetry-based Class E^2 WPT system are analytically derived.
3) The ZVS operation is quantitatively described for the PT-symmetry-based Class E^2 WPT system as a function of the equivalent phase of the PA and the coupling coefficient, indicating that the maximum phase variation with coupling coefficient is rather small and independent of the natural resonant frequency, so that the system output remains approximately constant.
4) A control circuit with current feedback and an appropriate phase shift is given to guarantee the PT mechanism and ZVS.

The rest of this article is organized as follows. In Section II, the coupled-mode theory (CMT) model of the PT-symmetry-based WPT system is analyzed. Section III presents the system structure, proposes a general design procedure for the PT-symmetry-based Class E^2 WPT system, and analytically derives the power losses and efficiencies of each component. The ZVS operation is quantitatively described as a function of the equivalent phase of the Class E PA and the coupling coefficient, and the PT symmetry principle for Class E^2 is analyzed in Section IV. Section V builds a prototype to validate the theoretical analysis and design. Finally, Section VI concludes this article.

II. CMT Modeling of the PT-Symmetry-Based WPT System

The CMT model of the PT-symmetry-based WPT system is shown in Fig. 1. The transmitter side makes up the gain circuit, and the receiver side composes the loss circuit. Here, L_i, C_i, and R_i ($i = 1, 2$), respectively, represent the self-inductances, tuning capacitances, and equivalent series resistances (ESRs) of the transmitting and receiving coils. κ represents the coupling coefficient between the two coils, and they share the same natural resonant frequency $\omega_1 = \omega_2 = \omega_0$. $-R'$ denotes the equivalent negative resistance of the gain circuit that provides energy for the system, and R_R refers to the equivalent load resistance of the loss circuit.

In the PT-symmetry-based WPT system, the parity reversal operation is the mirror symmetry of the spatial coordinates from the transmitting coil L_1 to the receiving coil L_2. The time-reversal operation is the conservation of energy emitted by the negative resistance $-R'$ in the gain circuit and absorbed by the load R_R in the loss circuit. The output voltage of the negative resistance $-R'$ is in the same phase as the output current, which means that the negative resistance $-R'$ can be equivalent to a power source. This characteristic of the negative resistance $-R'$ is the key to balancing gain and loss in the PT-symmetry-based WPT system.

Introducing complex variables

$$\boldsymbol{a_i} = A_i \, \mathrm{e}^{j(\omega t+\theta_i)} \tag{1}$$

where $|\boldsymbol{a_i}|^2$ ($i = 1, 2$), respectively, symbolize the energy in the transmitter and receiver resonators. A_i and θ_i are the amplitude and phase of $\boldsymbol{a_i}$, respectively, both of which vary slowly with time, giving the possibility of dynamic modeling [21].

The gain saturation mechanism of tracking PT symmetry is analyzed as follows. At the outset, there is little energy $|\boldsymbol{a}_1|^2$ contained in the transmitter resonator. The negative resistance $-R'$ feeds energy to the resonator tank that is then consumed by the load R_R, setting off an exponential increase in $|\boldsymbol{a}_1|^2$. With the growth of $|\boldsymbol{a}_1|^2$, the negative resistance $-R'$ converts into a positive resistance that absorbs the excess energy, giving rise to an exponential reduction of $|\boldsymbol{a}_1|^2$. Once $|\boldsymbol{a}_1|^2$ decreases, $-R'$ repeats the above-mentioned process until the gain balances out the loss, and the PT symmetry is thereof automatically tracked.

The dynamic equations of the CMT model can be described as follows [17], [18]:

$$\begin{bmatrix} \dot{\boldsymbol{a}}_1 \\ \dot{\boldsymbol{a}}_2 \end{bmatrix} = \begin{bmatrix} j\left(1+\frac{1}{1-\kappa^2}\right)\frac{\omega_0}{2}+\frac{g_1}{1-\kappa^2} & \frac{\kappa}{1-\kappa^2}\gamma_2 - j\frac{\kappa}{1-\kappa^2}\frac{\omega_0}{2} \\ \frac{\kappa}{1-\kappa^2}g_1 - j\frac{\kappa}{1-\kappa^2}\frac{\omega_0}{2} & j\left(1+\frac{1}{1-\kappa^2}\right)\frac{\omega_0}{2}-\frac{\gamma_2}{1-\kappa^2} \end{bmatrix} \begin{bmatrix} \boldsymbol{a}_1 \\ \boldsymbol{a}_2 \end{bmatrix} \tag{2}$$

where $\omega_0 = 1/\sqrt{L_2C_2}$ defines the natural resonant frequency, $g_1 = g_{10} - \gamma_{10} = 2U_s/(\pi\sqrt{2L_1}) - R_1/2L_1$ characterizes the gain rate of the transmitter resonator, and $\gamma_2 = \gamma_{20} + \gamma_R = R_2/2L_2 + R_R/2L_2$ represents the loss rate of the receiver resonator. The PT-symmetric conditions are as follows: $g_1 = \gamma_2$ and $\omega_1 = \omega_2 = \omega_0$.

By neglecting the second-order terms (κ has a relativelysmall but nonzero value), the dynamic (2) can be simplified as follows:

$$\begin{bmatrix} \dot{\boldsymbol{a}}_1 \\ \dot{\boldsymbol{a}}_2 \end{bmatrix} = \begin{bmatrix} j\omega_0 + g_1 & -j\frac{\omega_0}{2}\kappa \\ -j\frac{\omega_0}{2}\kappa & j\omega_0 - \gamma_2 \end{bmatrix} \begin{bmatrix} \boldsymbol{a}_1 \\ \boldsymbol{a}_2 \end{bmatrix}. \tag{3}$$

From (3), we get the following characteristic equation:

$$\begin{vmatrix} j(\omega-\omega_0)+g_1 & j\frac{\omega_0}{2}\kappa \\ j\frac{\omega_0}{2}\kappa & j(\omega-\omega_0)-\gamma_2 \end{vmatrix} = 0 \tag{4}$$

where ω denotes the operating frequency.

Then, by separating the imaginary and real parts of (4), the following is expressed:

$$\begin{cases} (\omega-\omega_0)^2 + g_1\lambda_2 - \frac{\omega^2k^2}{4} = 0 \\ (\omega-\omega_0)(g_1-\lambda_2) = 0 \end{cases}. \tag{5}$$

Then, the steady solutions with ω can be solved according to (5) as follows:

$$\omega = \begin{cases} \omega_0 \pm \sqrt{\frac{\omega_0^2}{4}\kappa^2 - \gamma_2^2}, & \kappa \geq \frac{2}{\omega_0}\gamma_2 \\ \omega_0, & \kappa < \frac{2}{\omega_0}\gamma_2 \end{cases}. \tag{6}$$

The energy mode of the receiving resonator is expressed as follows:

$$|\boldsymbol{a}_2| = \frac{g_{10}}{\gamma_{10}+\gamma_2}|\boldsymbol{a}_1| = \begin{cases} |\boldsymbol{a}_1|, & \kappa \geq \frac{2}{\omega_0}\gamma_2 \\ \frac{g_{10}\frac{\omega_0}{2}\kappa}{\frac{\omega_0^2}{4}\kappa^2+\gamma_{10}\gamma_2}|\boldsymbol{a}_1|, & \kappa < \frac{2}{\omega_0}\gamma_2 \end{cases}. \tag{7}$$

As can be observed from (6) and (7), a bifurcation of the operating frequency occurs in the exact PT-symmetric region ($\kappa \geq 2\gamma_2/\omega_0$), resulting in symmetric energy distribution ($|\boldsymbol{a}_1| = |\boldsymbol{a}_2|$). However, in the broken PT-symmetric region ($\kappa < 2\gamma_2/\omega_0$), the system operates at the natural resonant frequency. In this situation, the gain is less than the loss, resulting in a waste of energy ($|\boldsymbol{a}_1| > |\boldsymbol{a}_2|$).

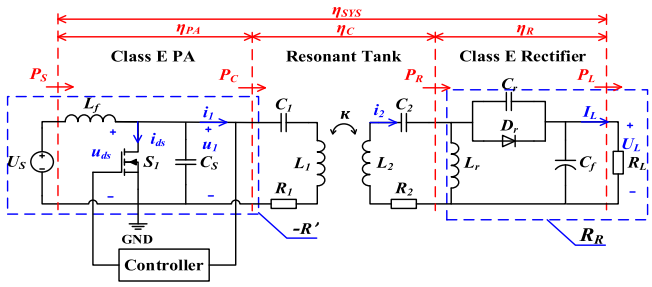

Fig. 2. General topology of the PT-symmetry-based Class E^2 WPT system.

The output power P_R and transfer efficiency η_C of the resonant tank are, respectively, derived as follows:

$$P_R = 2\gamma_R|\boldsymbol{a}_2|^2 = \begin{cases} \frac{2\gamma_R g_{10}^2|\boldsymbol{a}_1|^2}{(\gamma_{10}+\gamma_2)^2}, & \kappa \geq \frac{2}{\omega_0}\gamma_2 \\ \frac{2\gamma_R g_{10}^2|\boldsymbol{a}_1|^2\frac{\omega_0^2}{4}\kappa^2}{\left(\frac{\omega_0^2}{4}\kappa^2+\gamma_{10}\gamma_2\right)^2}, & \kappa < \frac{2}{\omega_0}\gamma_2 \end{cases} \tag{8}$$

$$\eta_C = \frac{2\gamma_R|\boldsymbol{a}_2|^2}{2\gamma_{10}|\boldsymbol{a}_1|^2+2\gamma_2|\boldsymbol{a}_2|^2} = \begin{cases} \frac{\gamma_R}{\gamma_{10}+\gamma_2}, & \kappa \geq \frac{2}{\omega_0}\gamma_2 \\ \frac{\gamma_R\frac{\omega_0^2}{4}\kappa^2}{\gamma_{10}\gamma_2^2+\gamma_2\frac{\omega_0^2}{4}\kappa^2}, & \kappa < \frac{2}{\omega_0}\gamma_2 \end{cases}. \tag{9}$$

Based on (8) and (9), it can be concluded that in the exact PT-symmetric region ($\kappa \geq 2\gamma_2/\omega_0$), both the output power P_R and transfer efficiency η_C of the resonant tank are irrelevant to the coupling coefficient κ. Since the ESRs of the transmitting and receiving coils R_1 and R_2 are well below the equivalent load resistance R_R, i.e., $(\gamma_{10}+\gamma_{20}) \ll \gamma_R$, robust and highly efficient power transfer is theoretically realizable.

III. Design Procedure for the PT-Symmetry-Based Class E^2 WPT System

Fig. 2 illustrates the general topology of the PT-symmetry-based Class E^2 WPT system, which contains a dc source, a Class E PA, a resonant tank, a Class E rectifier, a dc load, and a controller. The circuits in two blue dotted boxes could be equivalent to *–R'* and R_R, respectively, in Fig. 1. Provided the circuit works in $g_1 = \gamma_2$ and $\omega_1 = \omega_2 = \omega_0$, the PT-symmetric conditions could be satisfied.

Assuming P_S is the input power from the dc source, and P_L is the power received by the load. η_{PA}, η_C, and η_R represent the efficiencies of the Class E PA, resonant tank, and Class E rectifier, respectively.

The proposed design methodology for the PT-symmetry-based Class E^2 WPT system is a universal one, with any provided parameters of load resistance R_L, target output power P_L, and natural resonant frequency ω_0. The duty ratio D of both the switch in the PA and the diode in the rectifier is considered 0.5 for maximum power-output capability.

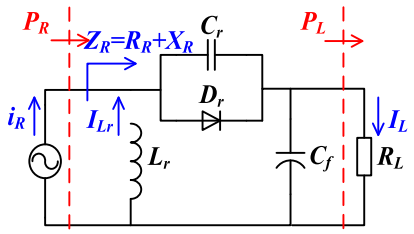

Fig. 3. Circuit model of the Class E rectifier.

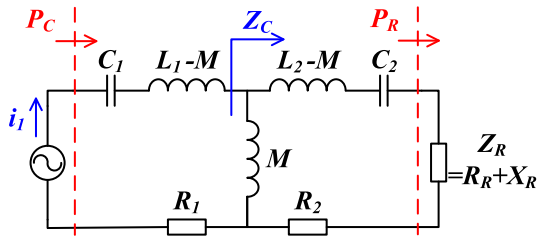

Fig. 4. Equivalent circuit model of the resonant tank.

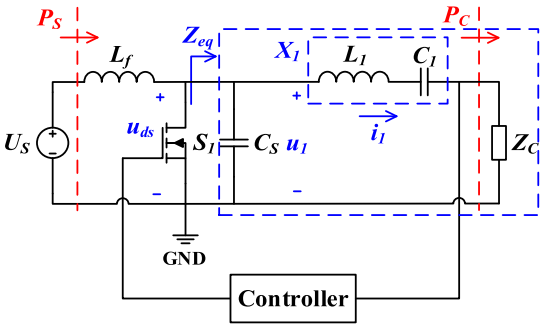

Fig. 5. Circuit model of the Class E PA.

A. Class E Rectifier

The Class E rectifier consists of a choke inductor L_r, a rectifying diode D_r, a shunt capacitor C_r, and a filter capacitor C_f. As can be seen in Fig. 3, the receiver resonator is ideally equivalent to a sinusoidal current source i_R, and the current through the choke inductor L_r equals the dc output current I_L. Therefore, to obtain a constant output current, the inductance L_r is required to be sufficiently large [22]. A large capacitance C_f is also needed for a small output voltage ripple [23].

According to Kazimierczuk [24], the solution for C_r is given as follows:

$$C_r = \frac{1}{\pi\omega_0(R_L + r_{Lr} + r_{Dr})} \tag{10}$$

where r_{Lr} denotes the ESR of the choke inductor L_r, and r_{Dr} refers to the ON-resistance of the diode D_r.

The input impedance Z_R of the rectifier can be represented by a series combination of a resistance R_R and a reactance X_R, which are, respectively, derived as follows:

$$R_R = \frac{8}{\pi^2+4}\left(R_L + r_{Lr} + \frac{\pi^2}{8}r_{Dr}\right) \tag{11}$$

$$X_R = -\frac{\pi\left(\pi^2-4\right)}{2(\pi^2+4)}\left[R_L + r_{Lr} + \frac{\pi^4-4\pi^2+16}{\pi^2\left(\pi^2-4\right)}r_{Dr}\right]. \tag{12}$$

The output current I_L is calculated as follows:

$$I_L = \sqrt{\frac{P_L}{R_L}}. \tag{13}$$

The input power P_R of the rectifier is thereof obtained as follows:

$$P_R = P_L + P_{Lr} + P_{Dr} \approx I_L^2\left(R_L + r_{Lr} + \frac{\pi^2}{8}r_{Dr}\right) \tag{14}$$

where P_{Lr} and P_{Dr} are the power losses on the chock inductor L_r and the diode D_r, respectively.

The efficiency η_R of the Class E rectifier is presented as follows:

$$\eta_R = \frac{P_L}{P_R} = \frac{R_L}{R_L + r_{Lr} + \frac{\pi^2}{8}r_{Dr}}. \tag{15}$$

B. Resonant Tank

Fig. 4 shows the equivalent circuit model of the resonant tank, where M characterizes the mutual inductance between L_1 and L_2, and Z_R denotes the input impedance of the rectifier.

Based on the equivalent circuit model shown in Fig. 4, the resonant equation of the receiver resonator is written as follows:

$$\omega_0 L_2 - \frac{1}{\omega_0 C_2} + X_R = 0. \tag{16}$$

Thus, the tuning capacitance C_2 is obtained as follows:

$$C_2 = \frac{1}{\omega_0(\omega_0 L_2 + X_R)}. \tag{17}$$

The mutual inductance M is given as follows:

$$M = \kappa\sqrt{L_1 L_2}. \tag{18}$$

In the broken PT-symmetric region, the operating frequency stays constant at ω_0, so that the equivalent reactance X_C of the receiving resonator is fully compensated by C_2. The equivalent resistance R_C of the receiving resonator can be calculated as follows:

$$R_C = R_1 + \frac{(\omega_0 M)^2}{R_R + R_2} = R_1 + \frac{\omega_0^2\kappa^2 L_1 L_2}{R_R + R_2}. \tag{19}$$

As the operating frequency ω adjusts with the change of the coupling coefficient κ in the exact PT-symmetric region, the equivalent impedance Z_S in the receiving resonator is no longer pure resistive. It can be expressed as follows:

$$Z_s = \mathrm{j}\left(\omega L_2 - \frac{1}{\omega C_2} + X_R\right) + (R_R + R_2). \tag{20}$$

Hence, the reflected impedance Z_C on the transferring side from the Z_S is now a combination of R_C and X_C, as

$$Z_C = \frac{\omega^2 M^2}{Z_s} = \frac{\omega^2\kappa^2 L_1 L_2}{Z_s} \tag{21}$$

$$\begin{cases} R_C = R_1 + \frac{\omega^2\kappa^2 L_1 L_2 (R_R+R_2)}{(R_R+R_2)^2 - \left(\omega L_2 - \frac{1}{\omega C_2} + X_R\right)^2} \\ \quad = R_1 + \frac{L_1}{L_2}(R_R + R_2) \\ X_C = -\frac{\omega^2\kappa^2 L_1 L_2 \left(\omega L_2 - \frac{1}{\omega C_2} + X_R\right)}{(R_R+R_2)^2 - \left(\omega L_2 - \frac{1}{\omega C_2} + X_R\right)^2} \\ \quad = L_1 \left[\frac{\pm 2\omega_0 \sqrt{\frac{\omega_0^2}{4}\kappa^2 - \gamma_2^2 + \frac{\omega_0^2}{4}\kappa^2 - \gamma_2^2}}{\omega_0^2 \pm \sqrt{\frac{\omega_0^2}{4}\kappa^2 - \gamma_2^2}}\right] \end{cases} . \quad (22)$$

From (21) and (22), it can be seen that the equivalent resistance R_C is a fixed value, whereas the equivalent reactance X_C depends on the coupling coefficient.

The transfer efficiency η_C of the resonant tank is expressed as follows:

$$\eta_C = \frac{P_R}{P_C} = \begin{cases} \frac{R_R}{\frac{L_2}{L_1}R_1 + R_R + R_2}, & \kappa \geq \frac{R_R+R_2}{\omega_0 L_2} \\ \frac{\omega_0^2\kappa^2 L_1 L_2 R_R}{R_1(R_R+R_2)^2 + (R_R+R_2)\omega_0^2\kappa^2 L_1 L_2}, & \kappa < \frac{R_R+R_2}{\omega_0 L_2} \end{cases} \quad (23)$$

$$\begin{cases} R_C = R_1 + \frac{\omega^2\kappa^2 L_1 L_2 (R_R+R_2)}{(R_R+R_2)^2 - \left(\omega L_2 - \frac{1}{\omega C_2} + X_R\right)^2} \\ \quad = R_1 + \frac{L_1}{L_2}(R_R + R_2) \\ X_C = -\frac{\omega^2\kappa^2 L_1 L_2 \left(\omega L_2 - \frac{1}{\omega C_2} + X_R\right)}{(R_R+R_2)^2 - \left(\omega L_2 - \frac{1}{\omega C_2} + X_R\right)^2} \\ \quad = L_1 \left[\frac{\pm 2\omega_0 \sqrt{\frac{\omega_0^2}{4}\kappa^2 - \gamma_2^2 + \frac{\omega_0^2}{4}\kappa^2 - \gamma_2^2}}{\omega_0^2 \pm \sqrt{\frac{\omega_0^2}{4}\kappa^2 - \gamma_2^2}}\right] \end{cases}$$

which is equivalent to (9).

Therefore, the input power P_C of the resonant tank can be presented as follows:

$$P_C = \frac{P_R}{\eta_C} . \quad (24)$$

C. Class E PA

As is depicted in Fig. 5, the Class E PA is comprised of a choke inductor L_f, a bidirectional switch S_1, a shunt capacitor C_S, and a series of resonance L_1C_1. Z_C refers to the equivalent impedance of the receiver resonator. The loaded quality factor Q_1 of the series resonance L_1C_1 is presumed to be sufficiently high, so the reactance X_1 is rather small at the natural resonant frequency ω_0 and large enough at higher harmonics to constrain the output current i_1 of the PA, i.e., the current of the transmitter resonator to be purely sinusoidal at ω_0 [20].

According to Kazimierczuk [24], Q_1, C_1, and C_S can be, respectively, designed by the following equations:

$$Q_1 = \frac{\omega_0 L_1}{R_C} \quad (25)$$

$$C_1 = \frac{1}{\omega_0 R_C \left[Q_1 - \frac{\pi(\pi^2-4)}{16}\right]} \quad (26)$$

$$C_S = \frac{8}{\pi(\pi^2+4)\omega_0 R_C} . \quad (27)$$

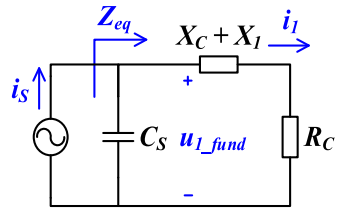

Fig. 6. Equivalent circuit model of the Class E PA ($u_{1\cdot\mathrm{fund}}$ denotes the fundamental of u_1).

In the broken PT-symmetric region, the series reactance X_1 is calculated as follows:

$$X_1 = \omega_0 L_1 - \frac{1}{\omega_0 C_1} = \frac{\pi(\pi^2-4)}{16} R_C . \quad (28)$$

However, in the exact PT-symmetric region, the series reactance X_1 is no longer constant, as

$$X_1 = \omega L_1 - \frac{1}{\omega C_1} = \frac{\pi(\pi^2-4)}{16} R_C \pm X_C \quad (29)$$

whereas $X_C + X_1$is independent of the coupling coefficient, as

$$X_C + X_1 = \frac{\pi(\pi^2-4)}{16} R_C . \quad (30)$$

Fig. 6 displays the equivalent circuit model of the Class E PA shown in Fig. 5. A current source i_S replaces U_S, L_f, and S_1, whereas C_S, $X_C + X_1$, and R_C form the resonant circuit. The equivalent impedance Z_{eq} of the PA is given as follows:

$$Z_{eq} = \frac{1}{j\omega C_S} //[R_C + j(X_C + X_1)]. \quad (31)$$

The phase of the equivalent impedance ϕ_{eq} can be deduced as follows:

$$\phi_{eq} = \arctan\left[-\frac{(X_C+X_1)^2 - (X_C+X_1)\frac{1}{\omega C_S} + R_C^2}{\frac{R_C}{\omega C_S}}\right] . \quad (32)$$

The minimum value of the choke inductance $L_{f\min}$ required to ignore the ac ripple on the input current is given as follows [24]:

$$L_{f\min} = 2\left(\frac{\pi^2}{4} + 1\right)\frac{R_C}{f_0} . \quad (33)$$

The input current I_S and input voltage U_S of the PA are, respectively, calculated as follows:

$$I_S = \frac{8}{\pi^2+4}\frac{U_S}{R_C} \quad (34)$$

$$U_S = \sqrt{\frac{\pi^2+4}{8} P_C R_C} . \quad (35)$$

The input power P_S of the PA is obtained as follows:

$$\begin{aligned} P_S &= P_C + P_{Lf} + P_{DS} + P_{\mathrm{tf}} \\ &= \frac{\pi^2+4}{8} I_S^2 \left[R_C + \frac{8}{\pi^2+4} r_{Lf} + \frac{\pi^2+28}{2(\pi^2+4)} r_{DS}\right] + \frac{(\omega t_f)^2 P_C}{12} \end{aligned} \quad (36)$$

where P_{Lf} is the power losses owing to the ESR of the chock inductor L_f. P_{DS} and $P_{\rm tf}$ are the conduction loss and turn-OFF loss on the switch S_1, respectively.

Hence, the efficiency $\eta_{\rm PA}$ of the Class E PA can be presented as follows:

$$\eta_{\rm PA} = \frac{P_C}{P_S} = \frac{R_C}{R_C + \frac{(\omega t_f)^2 R_C}{12} + \frac{8}{\pi^2+4} r_{Lf} + \frac{\pi^2+28}{2(\pi^2+4)} r_{DS}}. \tag{37}$$

As can be summarized in (9), (15), (23), and (37), when operating in the exact PT-symmetric region, the system efficiency $\eta_{\rm SYS}$ is a constant value determined only by the load R_L and the intrinsic parameters of the selected components.

IV. ZVS Operation Analysis and PT-Symmetry Principle Analysis

The principle of the ZVS operation is that the bidirectional switch S_1 of the Class E PA turns ON at zero voltage, leading to zero switching loss and thus high efficiency. The derivative of the drain-to-source voltage $du_{\rm DS}/d(\omega t)$ of the switch must be less than or equal to zero when the switch turns ON, i.e., the switch turns ON with the current through the shunt capacitor declining, implying that the switch current gradually rises from zero or negative after the switch is ON.

When the switch S_1 in the PA turns ON at $\omega t = 2\pi$, the ZVS condition is satisfied at [24]

$$u_{\rm DS}\ (2\pi) = 0 \tag{38}$$

and

$$\left.\frac{du_{\rm DS}}{d(\omega t)}\right|_{\omega t = 2\pi} \le 0. \tag{39}$$

A. Derivative of the Drain-to-Source Voltage

The output current i_1 of the PA is given as follows:

$$i_1 = I_m \sin(\omega t + \phi) \tag{40}$$

where I_m stands for the amplitude of i_1. ϕ denotes the phase difference between i_1 and the output voltage u_1 of the PA.

The drain-to-source voltage $u_{\rm DS}$ of the switch is given as follows [9], [25]:

$$u_{\rm DS} = \frac{1}{\omega C_s}\left[I_S \omega t + I_m \cos(\omega t + \phi) - I_m \cos\phi\right]. \tag{41}$$

By differentiating (41), we can obtain the following:

$$\frac{du_{\rm DS}}{d(\omega t)} = \frac{1}{\omega C_s}\left[I_S - I_m \sin(\omega t + \phi)\right]. \tag{42}$$

The amplitude of the resonant current I_m is given as follows [9], [25]:

$$I_m = \frac{4U_S}{\pi R_C}\cos\phi. \tag{43}$$

Imposing (38) into (41), a relationship among I_S, I_m, and ϕ is found as follows:

$$I_S = \frac{2}{\pi}\cos\phi I_m \tag{44}$$

TABLE I
Parameters of the Experimental Prototype

f_0	U_S	L_1	L_2	C_S
200 kHz	100 V	57.8 μH	58.4 μH	10 nF
C_1	C_2	C_r	r_{Lf}	r_{DS}
15.4 nF	14.2 nF	10 nF	0.3 Ω	0.08 Ω
R_1	R_2	r_{Lr}	r_{Dr}	R_L
0.124 Ω	0.129 Ω	0.4 Ω	0.024 Ω	25 Ω
L_f	L_r	P_R	κ_C	
2.5 mH	1 mH	165 W	0.17	

Substituting (43) and (44) into (42) yields the following:

$$\frac{du_{\rm DS}}{d(\omega t)} = \frac{4U_S}{\omega C_s \pi R_C}\cos\phi\left[\frac{2}{\pi}\cos\phi - \sin(\omega t + \phi)\right] \tag{45}$$

Substituting $\omega t = 2\pi$ into (45), we get the following:

$$\left.\frac{du_{\rm DS}}{d(\omega t)}\right|_{\omega t = 2\pi} = \frac{4U_S}{\omega C_s \pi R_C}\cos^2\phi\left[\frac{2}{\pi} - \tan\phi\right]. \tag{46}$$

Using the condition $du_{\rm DS}/d(\omega t)|_{\omega t = 2\pi} = 0$, the optimum phase lead $\phi_{\rm opt}$ of the output current i_1 relative to the output voltage u_1 of the PA is calculated as follows:

$$\phi_{\rm opt} = \arctan\frac{2}{\pi} = 32.48^\circ. \tag{47}$$

From (46), it can be deduced that the ZVS condition is satisfied at $\phi \ge \phi_{\rm opt}$.

B. Equivalent Phase of the PA in the PT-Symmetry-Based Class E^2 WPT System

The critical coupling coefficient κ_C is given as follows:

$$\kappa_C = \frac{2\gamma_2}{\omega_0} = \frac{R_R + R_2}{\omega_0 L_2}. \tag{48}$$

As can be noticed from (47), κ_C is in reverse proportion to the natural resonant frequency ω_0. Three different natural resonant frequencies $f_0 =$ 190, 200, and 210 kHz are, respectively, imposed into (5), giving three sets of operating frequencies f. As depicted in Fig. 7(a), with the increase in f_0, κ_C decreases, which is consistent with (48).

Fig. 7(b) displays the equivalent phase $\phi_{\rm eq}$ as a function of the coupling coefficient κ that was deduced in (32) (the utilized parameters are the same as those given in Table I, $\phi_{\rm eq}$reaches $\phi_{\rm opt}$ at the critical coupling coefficient). Two examples $f_0 =$ 200 kHz and 500 kHz are given in Fig. 8. The critical coupling coefficients κ_C are 0.2 and 0.08, respectively. From the figure, the condition $\phi_{\rm eq} \ge \phi_{\rm opt}$ is satisfied, i.e., ZVS operation is achieved when the system operates in the broken PT-symmetric region or the lower branch of ω in the exact PT-symmetric region. It can also be seen that the maximum phase variation with coupling coefficient ($\approx 3.5^\circ$) is independent of the natural resonant frequency ω_0.

C. PT-symmetry Principle for Class E^2 WPT

The Class E PA works as a nonlinear controlled source with equivalent nonlinear negative resistor $-R'$. Note that the class E

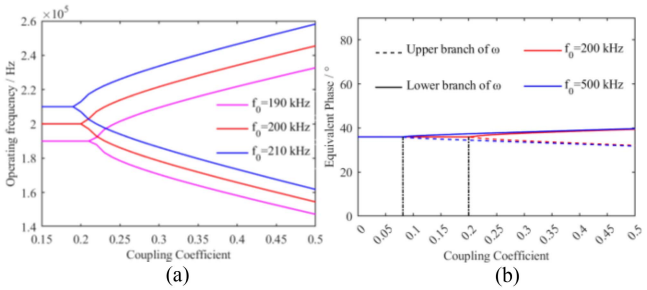

Fig. 7. (a) Operating frequency f concerning coupling coefficient κ. (b) Equivalent phase ϕ_{eq} as a function of coupling coefficient κ.

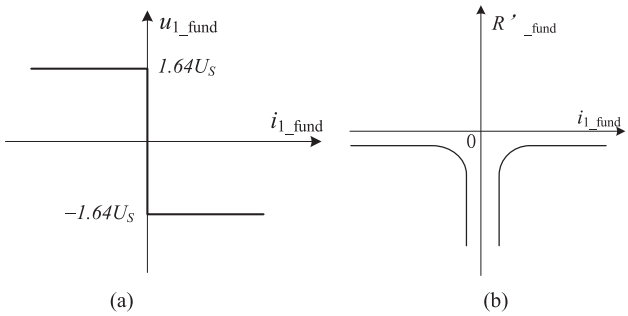

Fig. 8. Fundamental component characteristics of Class E PA. (a) Voltage–current characteristic. (b) Negative resistance characteristics.

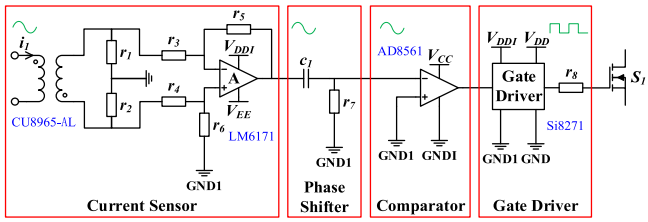

Fig. 9. Controller of the PT-symmetry-based Class E^2 WPT system.

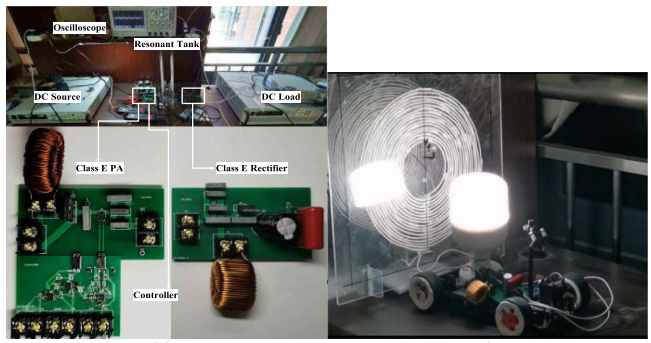

Fig. 10. Experimental prototype. (a) Static experimental prototype. (b) Dynamic experimental prototype.

PA has a fixed equivalent resistor R_R as (11). When the energy increases to infinity on the transmitting side, the R' trends to be saturation value 0. Hence, the proposed Class E^2 WPT could work in a PT-symmetry eigenmode automatically. Assuming the output current i_1 of the PA is given by (40), then it yields the following:

$$\frac{u_1}{U_S}=\begin{cases}0 & \text{for } 0<\omega t\le 2\pi D\\ \frac{\tan(\pi D+\phi)\sin\pi D}{(1-D)[\pi(1-D)\cos\pi D+\sin\pi D]}\{\omega t-2\pi D & \\ \quad+\frac{2\pi(1-D)}{\cos(2\pi D+\phi)-\cos\phi}[\cos(\omega t+\phi) & \\ \quad-\cos(2\pi D+\phi)]\}, & \text{for } 2\pi D<\omega t\le 2\pi\end{cases} \tag{49}$$

$$\phi=\pi+\arctan\left[\frac{\cos 2\pi D-1}{2\pi(1-D)+\sin 2\pi D}\right]. \tag{50}$$

Considering $D=0.5$, then it yields

$$u_{1\_\text{fund}}=1.64U_S\sin(\omega t+\theta),\theta=\text{arctg}\left(\frac{\pi}{2}-\frac{4}{\pi}\right). \tag{51}$$

According to (51), the fundamental component characteristics of Class E PA are plotted in Fig. 7. As can be seen from Fig. 7(a), the fundamental voltage is limited to $\mp 1.64U_S$, and R' is negatively correlated with the transmitting resonator current. When the energy of the transmitting resonator tends to be infinity, R' becomes saturated, as shown in Fig. 7(b). Hence, the Class E^2 WPT could work in the eigenmode of PT symmetry.

V. Experimental Verification

Based on the above-mentioned analysis, an experimental prototype is implemented to practically evaluate the performance of the PT-symmetry-based Class E^2 WPT system.

A. Control Strategy

According to the gain saturation mechanism of tracking PT symmetry analyzed in Section II, by sampling only the current i_1 of the transmitting resonator, the output voltage u_1 and output current i_1 of the Class E PA can be controlled synchronously. The PA is thereof turned into a negative resistance, self-tracking the operating frequency to assure the satisfaction of PT symmetry.

The realization of the controller is on account of the circuit diagram shown in Fig. 9 . A current sense transformer CU8965-AL is used to sample the current i_1 of the transmitting resonator. Via a differential amplifying circuit that consists of an operational amplifier LM6171, the current i_1 is converted into a voltage signal and then sent to an *RC* phase shifter. Different from the previous work, the phase shifter is to offset the phase lead ϕ_{eq} of the current i_1 relative to the voltage $u_1$and to compensate for the phase shift from the control circuit, such that the Class E PA is locked in optimum or suboptimum operating conditions for ZVS. The zero-crossing points of the signal coming from the phase shifter are then detected by a comparator AD8561. Finally, a gate driver Si8271 receives the output to generate the gate driving signal U_{GS} of the switch S_1.

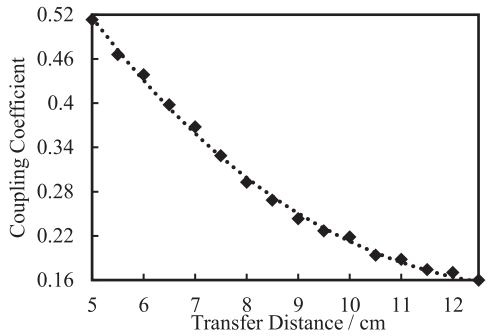

Fig. 11. Coupling coefficient κ concerning the transfer distance d between the two coils.

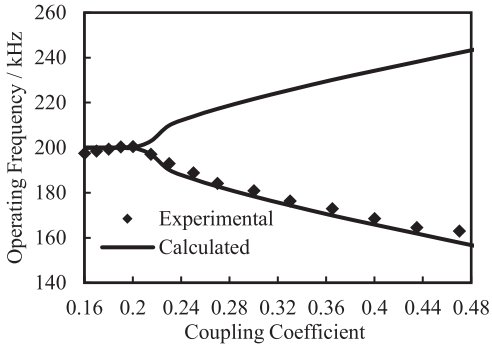

Fig. 12. Operating frequency f concerning coupling coefficient κ.

B. Experimental Setup

Fig. 10(a) displays a photograph of the experimental prototype, in which the switch S_1 utilizes a silicon carbide power MOSFET (C2M0080120D), and the rectifying diode D_r adopts a Schottky power diode (MBR40250G). Each coil L_i ($i = 1, 2$) has an inner diameter of 5 cm and an outer diameter of 15 cm, which is made by winding 16 turns of 500-strand wire on an acrylic plate. Table I lists the parameters applied. The variation of the coupling coefficient with the distance between the two coils is measured and drawn in Fig. 11. Determined by the parameters in Table I, the critical coupling coefficient κ_C is calculated as 0.17 according to (48). Fig. 10(b) displays the dynamic experimental prototype, where the receiving end is carried by an electric toy car.

The measurement approaches for the output power and system efficiency are given as follows. The input power P_S is directly read from the dc source. The output voltage U_L and current I_L are gauged by an oscilloscope. Finally, the output power is obtained using the relation $P_L = U_L \cdot I_L$, and the system efficiency is acquired by (9).

C. Experimental Results

The experimental and calculated operating frequencies f concerning the coupling coefficient κ are depicted in Fig. 12, showing the prototype operates in the lower branch of ω in the exact PT-symmetric region. The experimental results coincide with the calculated values.

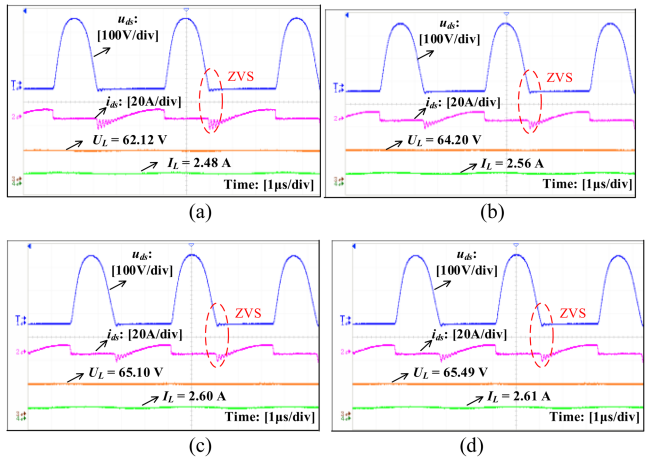

Fig. 13. Experimental waveforms of u_{ds}, i_{ds}, I_L, and U_L with various κ. (a) $\kappa = 0.17$, $d = 12$ cm. (b) $\kappa = 0.22$, $d = 10$ cm. (c) $\kappa = 0.32$, $d = 8$ cm; (d) $\kappa = 0.44$, $d = 6$ cm.

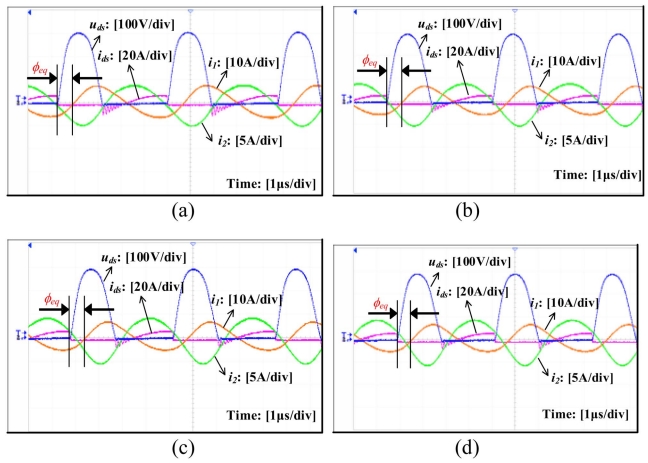

Fig. 14. Experimental waveforms of u_{ds}, i_{ds}, i_1, and i_2 with various κ. (a) $\kappa = 0.17$, $d = 12$ cm. (b) $\kappa = 0.22$, $d = 10$ cm. (c) $\kappa = 0.32$, $d = 8$ cm. (d) $\kappa = 0.44$, $d = 6$ cm.

Fig. 13 displays the experimental waveforms of the drain-to-source voltage $U_{\rm DS}$ and drain current I_D of the switch, output current I_L, and output voltage U_L under a series of coupling coefficients. The yellow waveform represents I_L, and the green waveform refers to U_L. In Fig. 13(b)–(d), $\kappa = 0.22$, 0.32, and 0.44, respectively, corresponding to the exact PT-symmetric region, and both I_L and U_L remain approximately the same. The realization of robust output power is thereof certified. However, in Fig. 13(a), $\kappa = 0.17$, i.e., in the broken PT-symmetric region, both I_L and U_L drop slightly, which corroborates the theoretical analysis presented in Sections II and III.

The experimental waveforms of u_{ds} and i_{ds} and resonant currents I_1 and I_2 of the transmitter and receiver resonators with various coupling coefficients are illustrated in Fig. 14. The blue and yellow waveforms, respectively, denote u_{ds} and i_1. It can be observed that the phase difference between u_{ds} and i_1, i.e., the equivalent phase $\phi_{\rm eq}$ of the PA, matches the theoretical result shown in Fig. 7(b). It is therefore proven that the applied

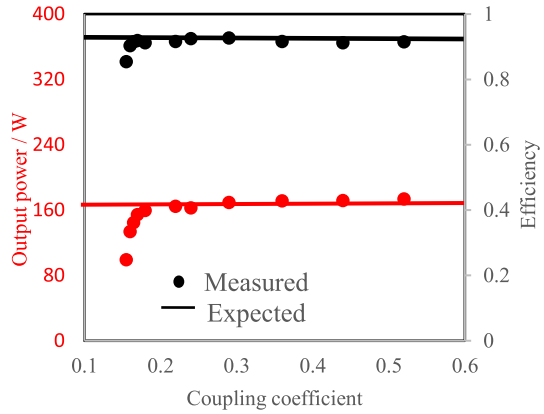

Fig. 15. Output power and system efficiency of the proposed Class E^2 WPT systems under different coupling coefficients (the red and black represent the output power and efficiency, respectively).

PT-symmetry-based control strategy is feasible for the Class E^2 WPT system.

The blue and pink waveforms in Figs. 13 and 14 represent u_{ds} and i_{ds}, respectively. It can be noticed that ZVS operation is achieved in both exact and broken PT-symmetric regions, which is overlapped with the quantitative description given in Section IV. Meanwhile, it suggests that the ZVS could be easier to be realized with the decreasing coupling coefficient κ since the equivalent phase ϕ_{eq} will become smaller at a low branch of ω, which is according to Fig. 7(b) as well. It is worth noting that there are oscillations in the current due to the presence of parasitic parameters.

Fig. 15 describes the output power and system efficiency of the proposed and typical Class E^2 WPT systems in a wide range of coupling coefficients. The expected 165 W of output power (various coupling coefficients) and 92.6% of system efficiency are respectively drawn with solid lines. The circles and triangles depict the experimental results of the proposed and typical systems, respectively. In the broken PT-symmetric region, output power and system efficiency of both proposed and typical systems drop with the decrease in the coupling coefficient, due to the invariant operating frequency. In the exact PT-symmetry region, output power and system efficiency of the typical system first stay roughly the same and then drop with the coupling coefficient increasing. By contrast, the proposed system ensures that the ZVS condition is reached for the sensitive Class E PA, even under the drastic variation of the coupling coefficient (from 0.17 to 0.47). As a result, robust and highly efficient power transfer is acquired for the PT-symmetry-based Class E^2 WPT system.

What is worth mentioning is that, as seen from (7) and (8), both output power P_R and transfer efficiency η_C of the resonant tank are theoretically irrelevant to the coupling coefficient κ in the exact PT-symmetric region ($\kappa \geq 2\gamma_2/\omega_0$). However, γ_{10} maybe a little different due to various operating frequencies. Hence, in practice, the transfer power and efficiency may have a few deviations.

Fig. 16(a) and (b) shows the dynamic waveforms of resonant current i_1, output current I_L, and output voltage U_L at a distance

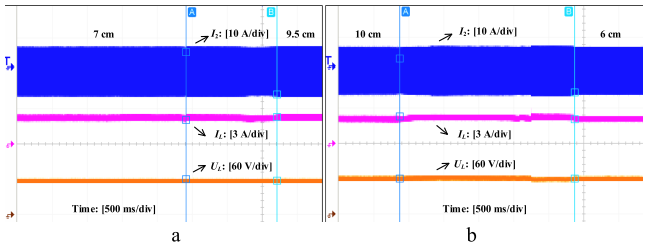

Fig. 16. Dynamic experimental waveforms of I_L, i_2, and U_L during moving. (a) d from 7 to 9.5 cm. (b) d from 10 to 6 cm.

TABLE II
EXISTING PT-SYMMETRY-BASED WPT SYSTEMS

Ref.	Inversion topology	Rectifier topology	Efficiency	Output Power (W)	Soft switching
[15]	operational amplifier	without	35%	0.0197	N
[16]	Half-bridge	without	83.7%	10	N
[17]	Full-bridge	Full-bridge	90%	150	N
[18]	Full-bridge	Full-bridge	91.9%	400	Y
[20]	E	without	92%	10	Y
Proposed	E	E	92.6%	165	Y

of 7–9.5 cm and 10–6 cm for the receiving end when the receiving coil moves at a speed of 2 cm/s. It can be seen that I_L, i_2, and U_L only fluctuate slightly when the distance changes from 7 to 9.5 cm and from 10 to 6 cm and remain unchanged. It is concluded that the E2-type WPT system based on PT symmetry can achieve excellent range robustness control.

Table II shows the comparison of the performances of some PT-symmetric WPT system prototypes published in recent years, such as system efficiency, output power, and soft switch. As can be seen from the table, the proposed E2 class WPT system based on PT symmetry proposed in this article has significant advantages due to its soft switching, high system efficiency, and simple control circuit. At higher output power, a greater efficiency advantage will be obtained.

VI. CONCLUSION

This article establishes a PT-symmetry-based Class E^2 WPT system for robust and highly efficient power transfer. The CMT modeling shows that when in the exact PT-symmetric region, both the output power and transfer efficiency of the PT-symmetry-based WPT system are independent of the coupling coefficient. A universal design methodology for the PT-symmetry-based Class E^2 WPT system is developed, guiding other WPT systems with mirror-symmetric oscillators between the transmitter and receiver. The power losses and efficiencies of each part of the system are analytically derived. For the first time, the ZVS operation is quantitatively described for the PT-symmetry-based Class E^2 WPT system as a function of the equivalent phase of the PA and the coupling coefficient, revealing that the maximum phase variation with coupling coefficient is rather small and independent of the natural resonant

frequency. The experimental results validate that a 165-W prototype can realize robust and highly efficient power transfer under the variation of the coupling coefficient.

REFERENCES

[1] A. Kurs, A. Karalis, R. Moffatt, J. D. Joannopoulos, P. Fisher, and M. Soljacic, "Wireless power transfer via strongly coupled magnetic resonances," *Science*, vol. 317, pp. 83–86, Jul. 2007.

[2] B. cheng and L. He, "High-order-network-based general modeling method for improved transfer performance," *IEEE Trans. Power Electron.*, vol. 36, no. 11, pp. 12375–12388, Nov. 2021.

[3] T. Nagashima et al., "Analytical design procedure for resonant inductively coupled wireless power transfer system with class-E^2 DC–DC converter," in *Proc. IEEE Int. Symp. Circuits Syst .*, 2014, pp. 113–116.

[4] M. Liu, M. Fu, and C. Ma, "Parameter design for a 6.78-MHz wireless power transfer system based on analytical derivation of class E current-driven rectifier," *IEEE Trans. Power Electron.*, vol. 31, no. 6, pp. 4280–4291, Jun. 2016.

[5] H. Sekiya et al., "Loosely coupled inductive wireless power transfer systems with class-E transmitter and multiple receivers," in *Proc. IEEE Energy Convers. Congr. Expo.*, 2014, pp. 675–680.

[6] W. Chen, R. A. Chinga, S. Yoshida, J. Lin, C. Chen, and W. Lo, "A 25.6 W 13.56 MHz wireless power transfer system with a 94% efficiency GaN class-E power amplifier," in *Proc. IEEE/MTT-S Int. Microw. Symp. Dig.*, 2012, pp. 1–3.

[7] D. C. Yates, S. Aldhaher, and P. D. Mitcheson, "A 100-W 94% efficient 6-MHz SiC class E inverter with a sub 2-W GaN resonant gate drive for IPT," in *Proc. IEEE Wireless Power Transfer Conf .*, 2016, pp. 1–3.

[8] T. Nagashima, X. Wei, E. Bou, E. Alarcón, M. K. Kazimierczuk, and H. Sekiya, "Steady-state analysis of isolated class-E^2 converter outside nominal operation," *IEEE Trans. Ind. Electron.*, vol. 64, no. 4, pp. 3227–3238, Apr. 2017.

[9] A. Ayachit, F. Corti, A. Reatti, and M. K. Kazimierczuk, "Zero-voltage switching operation of transformer class-E inverter at any coupling coefficient," *IEEE Trans. Ind. Electron.*, vol. 66, no. 3, pp. 1809–1819, Mar. 2019.

[10] M. Liu, J. Song, and C. Ma, "Active class E rectifier for DC output voltage regulation in megahertz wireless power transfer systems," *IEEE Trans. Ind. Electron.*, vol. 67, no. 5, pp. 3618–3628, May 2020.

[11] L. He and D. Guo, "An active switched-capacitor half-wave receiver with high efficiency and reduced components in WPT system," *IEEE Trans. Ind. Electron.*, vol. 68, no. 12, pp. 12119–12129, Dec. 2021.

[12] L. He and D. Guo, "A clamped and harmonic injected class-E converter with ZVS and reduced voltage stress over wide range of distance in WPT system," *IEEE Trans. Power Electron.*, vol. 36, no. 6, pp. 6339–6350, Jun. 2021.

[13] M. Liu, Y. Qiao, S. Liu, and C. Ma, "Analysis and design of a robust class E^2 DC–DC converter for megahertz wireless power transfer," *IEEE Trans. Power Electron.*, vol. 32, no. 4, pp. 2835–2845, Apr. 2017.

[14] S. Liu, M. Liu, S. Han, X. Zhu, and C. Ma, "Tunable class E^2 DC–DC converter with high efficiency and stable output power for 6.78-MHz wireless power transfer," *IEEE Trans. Power Electron.*, vol. 33, no. 8, pp. 6877–6886, Aug. 2018.

[15] S. Assawaworrarit, X. Yu, and S. Fan, "Robust wireless power transfer using a nonlinear parity–time-symmetric circuit," *Nature*, vol. 546, no. 7658, pp. 387–390, Jun. 2017.

[16] Y. Hou, M. Lin, W. Chen, and X. Yang, "Dual-coupled robust wireless power transfer based on parity–time-symmetric model," in *Proc. IEEE Int. Power Electron. Appl. Conf. Expo.*, 2018, pp. 1–5.

[17] J. Zhou, B. Zhang, W. Xiao, D. Qiu, and Y. Chen, "Nonlinear parity–time-symmetric model for constant efficiency wireless power transfer: Application to a drone-in-flight wireless charging platform," *IEEE Trans. Ind. Electron.*, vol. 66, no. 5, pp. 4097–4107, May 2019.

[18] Z. Zhang and B. Zhang, "Omnidirectional and efficient wireless power transfer system for logistic robots," *IEEE Access*, vol. 8, pp. 13683–13693, Jan. 2020.

[19] H. Zhu, B. Zhang, and L. Wu, "Output power stabilization for wireless power transfer system employing primary-side-only control," *IEEE Access*, vol. 8, pp. 63735–63747, Mar. 2020.

[20] S. Assawaworrarit and S. Fan, "Robust and efficient wireless power transfer using a switch-mode implementation of a nonlinear parity–time symmetric circuit," *Nature Electron.*, vol. 3, pp. 273–279, May 2020.

[21] H. Li, K. Wang, L. Huang, W. Chen, and X. Yang, "Dynamic modeling based on coupled modes for wireless power transfer systems," *IEEE Trans. Power Electron.*, vol. 30, no. 11, pp. 6245–6253, Nov. 2015.

[22] M. K. Kazimierczuk and W. Szaraniec, "Class D–E resonant DC/DC converter," *IEEE Trans. Aerosp. Electron. Syst.*, vol. 29, no. 3, pp. 963–976, Jul. 1993.

[23] J. J. Jozwik and M. K. Kazimierczuk, "Analysis and design of class-E^2 DC/DC converter," *IEEE Trans. Ind. Electron.*, vol. 37, no. 2, pp. 173–183, Apr. 1990.

[24] M. K. Kazimierczuk, *RF Power Amplifiers*. Hoboken, NJ: Wiley, 2008.

[25] B. Cheng, L. He, L. Li, H. Liu, and F. Lu, "Improved wireless power transfer system utilizing a rectifier with nonlinear resistance compression characteristic," *Appl. Energy*, vol. 311, Dec. 2022, Art. no. 120365.

Liangzong He (Member, IEEE) was born in Hunan, China, in 1984. He received the B.Sc. degree in power electronics from Jilin University, Changchun, China, in 2006, and the Ph.D. degree in electrical engineering from the Huazhong University of Science and Technology, Wuhan, China, in 2012.

From November 2009 to August 2011, he was a joint Ph.D. education student with Michigan State University, East Lansing, MI, USA. In September 2012, as an Assistant Professor, he joined Xiamen University, Xiamen, China, where he has been a Professor since August 2019. His research interests include high-efficient power conversion, wireless power transmission, stability analysis and low-frequency ripple suppression.

Xiayi Huang was born in Fuzhou, China, in 1999. He received the B.E. degree in power electronics from Xiamen University, Xiamen, China, in 2021. She is currently working toward the M.S. degree in power electronics at the Department of Electrical Engineering, Tongji University, Shanghai, China.

Her current research interest includes wireless power transfer.

Bing Cheng was born in Henan, China, in 1996. He received the B.E. degree in power electronics from Xiamen University, Xiamen, China, in 2018. He is currently working toward the Ph.D. degree in power electronics with the Department of Instrumental and Electrical Engineering, Xiamen University.

His research interests include modeling and control of wireless power transfer systems.